Supplementary Information:

A HoLDI mass spectrometry platform for airborne nanoplastic detection

Zi Wang[1], Nadim K. Saadé[1], Robert J. Panetta[1], and Parisa A. Ariya[1, 2*]

[1]Department of Chemistry, McGill University, Montreal, Quebec H3A 0B8, Canada, [2]Department of Atmospheric and Oceanic Sciences, McGill University, Montreal, Quebec H3A 0B9, Canada

*Correspondence to: Parisa A. Ariya, parisa.ariya@mcgill.ca

Glossary of terms

ATR: Attenuated total reflectance

CPE: Chlorinated polyethylene

DSC: Differential scanning calorimetry

EDS: Energy-dispersive spectroscopy

HDPE: High-density polyethylene

HEPA: High efficiency particulate air

HoLDI: Hollow-laser desorption/ionization

HR-TEM: High-resolution transmission electron microscopy

LC: Liquid chromatography

μFTIR: Micro-Fourier transform infrared spectroscopy

μRaman: Micro-Raman spectroscopy

LDIR: Laser direct infrared

LDPE: Low-density polyethylene

MALDI-TOF-MS: Matrix-assisted laser desorption/ionization time-of-flight mass spectrometry

MOUDI: Micro-orifice uniform deposit impactor

MS/MS: Tandem mass spectrometry

NTA: Nanoparticle tracking analyzer

OPS: Optical particle sizer

PA: Polyamide

PB: Polybutadiene

PC: Polycarbonate

PDMS: Polydimethylsiloxane

PE: Polyethylene

PEG: Polyethylene glycol

PES: Polyester

PET: Polyethylene terephthalate

PP: Polypropylene

PS: Polystyrene

PUR: Polyurethane

PVA: Polyvinyl alcohol

PVC: Polyvinyl chloride

PVDF: Polyvinylidene fluoride

Pyr-GC-MS: Pyrolysis gas chromatography mass spectrometry

QQQ-ICP-MS/MS: Triple quadrupole inductively coupled plasma tandem mass spectrometry

SMPS: Scanning mobility particle sizer

TD-PTR-MS: Thermal desorption proton-transfer-reaction mass spectroscopy

TEM: Transmission electron microscopy

THF: Tetrahydrofuran

TOC: Total organic carbon

UV: Ultraviolet

Table S1 | A comparison of selected environmental nano/microplastic research carried out using various sample collection approaches, preparation methods, and major analytical techniques.

Environmental matrix and sampling site			Sample collection	Sample preparation	Analytical technique	Plastic detected	Ref.
Air	Suspended aerosol	Within and above the planetary boundary layer over urban and rural areas, Spain	Onto stainless-steel filters by a vacuum pump, on an airplane	Not applied	μ-FTIR	PA, PB, PE, PES, PP, PUR, and acrylic; 1.5 particles·m^{-3} (rural) - 13.9 particles·m^{-3} (urban)	[1]
		Marine atmosphere, North Atlantic Ocean	Onto polycarbonate filters by a vacuum pump	Not applied	μ-Raman	PDMS, PE, PP, and PS; ~ 0.01 - 0.1 particles·m^{-3}	[2]
	Dry deposition	Domestic indoor dust, Netherlands	Into glass bottles from vacuum cleaner	In-matrix depolymerization and filtration	LC-UV	PET; 1.2 - 305 mg·g^{-1}	[3]
		Outdoor dust from windowsills and open-air balconies, major cities, China	Into paper bags with aluminium foil lining, using hog bristle brushes	Visual sorting, sieving, depolymerization, extraction, spiking, solid-phase extraction, and re-dissolving	LC-MS/MS	PC (2.0 mg·kg^{-1}) and PET (212 - 9020 mg·kg^{-1})	[4]
	Wet deposition	Rainwater in an urban area, China	Into glass containers	Filtration, ultrasonication, digestion, and evaporation	μ-Raman	PS and PVC; 0.28 % - 0.40 %	[5]
		Fresh and aged snow, urban area, Canada	Into glass jars with a scope	Melting and homogenization	MALDI-TOF-MS	PE (> 100 ng·mL^{-1}) and PEG (21.9 ng·mL^{-1})	[6]
Water	River	Surface water, Rhine River	Via a manta net from vessels	Rinsing, sieving, digestion, density separation, and visual sorting	ATR-FTIR	PES, PP, PS, PVC, and acrylate; 892777 particles·km^{-2}	[7]
		Gallatin River watershed, USA	Into stainless-steel bottles using a grab	Filtration, drying, visual inspection, and hot needle test	μ-FTIR	PA, PES, PET, PP, PVA, PVDF, poly(trimellitamide	[8]

			approach; or wading and using a sampling pole			imide), acrylic, butyl rubber, neoprene, and semi-synthetic cellulose; 1.2 particles·L^{-1}	
	Lake	Surface water, western Lake Superior	Via a manta net and a collection vessel	Sieving, washing, digestion, density separation, filtration, and drying	Pyr-GC-MS and ATR-FTIR	PE, PET, PDMS, PP, PS, PVC, CPE, and dodecyl phthalate resin; 91 - 3538 mg·km^{-2} (0 - 110000 particles·km^{-2})	[9]
		Surface water, lake Gårdsjön, Sweden	Into glass bottles by hand	Filtration	TD-PTR-MS	PE, PET, PP, and PVC; 563 µg·L^{-1}	[10]
	Ocean	Surface layer seawater, subtropical gyre, western North Atlantic Ocean	Manta nets and glass bottles, on a sailing vessel	Agitation, digestion, filtration, ultrafiltration, freeze-drying, and homogenization	Pyr-GC-MS and µ-FTIR	PE, PET, PP, PS, and PVC; 500000 - 7000000 particles·km^{-2}	[11]
		The southernmost of the Tyrrhenian Sea	By a Bongo net	Visual sorting, washing, and centrifugation	Raman and ATR-FTIR	LDPE and PVC	[12]
	Ground-water	Unconfined groundwater aquifer, Bacchus Marsh, Australia	Into glass bottles, by a stainless-steel bailer with a braided polyamide rope	Filtration, digestion, and density separation	LDIR	PA, PC, PE, PET, PMMA, PP, PS, and PVC; 16 - 97 particles·L^{-1}	[13]
		Karst aquifers, Illinois, USA	Into HDPE bottles and glass bottles	Filtration, drying, and visual inspection	Pyr-GC-MS	PE; 0 - 15.2 particles·L^{-1}	[14]
Soil and sediment	Industrial soil	Soil near an industrial site, Australia	Not specified	Drying, sieving, pressurized fluid extraction, and evaporation	ATR-FTIR	PE, PS, and PVC; 0.03% - 6.7%	[15]

		Soil of Ahvaz metropolis, Iran	Into glass jars by a stainless-steel shovel	Drying, manual sorting, sieving, digestion, and floatation	μ-Raman	PP, PS, PET, and nylon; 80 - 1220 pieces·kg^{-1}	[16]
	Agricultural field	Agricultural soil, Chilean central valley, Chile	Collected using a metallic soil auger and stored in PP plastic bags	Drying, sieving, and wet extraction (i.e., floatation, stirring, centrifugation, and filtration cycles)	Stereo microscope (visual inspection)	Fibers, films, pellets, and fragments; 0.6 - 10.4 pieces·g^{-1}	[17]
		Highly contaminated agricultural soil, central France	Not specified	Drying, sieving, water extraction, filtration, and fractionation	Pyr-GC-MS	PE, PS, and PVC	[18]
	Sand	Beach sand from El Quetzalito Beach, Guatemala	Into aluminum trays using a stainless-steel spatula	Drying, sieving, and density separation	ATR-FTIR	PE, PP, and PS; 279 pieces·m^{-2} (30 pieces·kg^{-1})	[19]
		Beach sand along the South Korean coast, Korea	Scooped and sieved into PE bottles	Sieving, homogenization, extraction, density separation, drying, and digestion	μ-FTIR	PE, PES, PP, PS, polyether urethane, poly(vinyls), poly(lauryl acrylate), and phenoxy resin; 1400 - 62800 pieces·m^{-2}	[20]
	Sediment	Upper River Tame catchment, UK	Collected using a stainless-steel scoop	Wet sieving, rinsing, drying, floatation, and visual sorting	ATR-FTIR	PE, PVC, and acrylic; 165 particles·kg^{-1}	[21]
		St. Lawrence River, Canada	Collected using a petite Ponar grab and a single Peterson grab	Sieving	Stereo microscope (visual inspection) and DSC	PE microbeads; 13832 microbeads·m^{-2}	[22]

Table S2 | 3D-printed matrix-assisted laser desorption/ionization (MALDI) target plates for mass spectrometry analysis of various analytes.

Description	Configuration adopted	Printing material	Analyte	Ref.
96 sample spots, with a 10 µL reservoir	MBT Biotarget 96 (Bruker Daltonics)	Conductive acrylonitrile butadiene styrene with carbon particles	Proteins and peptides	[23]
96 sample spots, matrix-free	MSP 96 Target (Bruker Daltonics)	Graphene-doped photocurable resin	Low-mass environmental pollutants and biological molecules	[24]
Hollow configurations, in combination with substrates	Prespotted AnchorChip 96 and MSP 96 NALDI Target (Burker Daltonics)	Electrically conductive polylactic acid, can be replaced by other materials	Environmental nano- and microplastics	This work

Table S3 | Conductivity measurements of different MALDI plates, including the 3D-printed HoLDI plate developed in this work, Bruker Daltonics's Prespotted AnchorChip 96 target made from conductive polymer, and Bruker Daltonics's stainless-steel MSP 96 NALDI target. Conductivity is calculated using Equation (1) in Methods, with sheet resistance measured via a four-point probe.

	HoLDI Target Plate	Prespotted AnchorChip 96 Target (Bruker Daltonics)	MSP 96 NALDI Target (Bruker Daltonics)
Sheet resistance ($\Omega \cdot sq^{-1}$)	2.27×10^{2}	4.93×10^{1}	2.97×10^{0}
Thickness (m)	8.50×10^{-4}	1.42×10^{-3}	8.50×10^{-4}
Conductivity ($S \cdot m^{-1}$)	5.40×10^{0}	1.80×10^{1}	4.13×10^{2}

Table S4 | Metal analysis of nano-sized airborne particles collected in (a) an indoor public space and (b) an outdoor environment. Concentrations are derived from reverse calculations based on Equation (4) in the Methods section, representing the mass of metals in the total volume of air passed through each stage of the impactor. The values are reported in ppb, with standard deviations in parentheses. Measurements < 0.000 ppb by ICP-MS prior to reverse calculations are denoted as "ND" (not detected).

(a)	Stage 6 – 1.0 µm	Stage 7 – 0.56 µm	Stage 8 – 0.31 µm	Stage 9 – 0.18 µm
Na	5.78×10^{-7} (6.42×10^{-8})	5.89×10^{-7} (1.89×10^{-8})	5.56×10^{-7} (2.45×10^{-8})	5.78×10^{-7} (2.49×10^{-8})
Al	ND	ND	ND	ND
K	ND	ND	ND	ND
V	2.34×10^{-6} (2.34×10^{-9})	2.36×10^{-6} (7.06×10^{-9})	2.34×10^{-6} (2.34×10^{-9})	2.34×10^{-6} (2.34×10^{-9})
Cr	ND	ND	ND	ND
Mn	ND	ND	ND	ND
Fe	ND	ND	ND	ND
Ni	1.96×10^{-5} (4.10×10^{-7})	1.15×10^{-5} (2.64×10^{-7})	1.25×10^{-5} (8.72×10^{-8})	1.18×10^{-5} (3.78×10^{-7})
Zn	ND	ND	ND	ND
As	5.78×10^{-7} (5.20×10^{-9})	4.67×10^{-7} (3.13×10^{-8})	4.33×10^{-7} (1.74×10^{-8})	4.33×10^{-7} (1.47×10^{-8})
Se	1.89×10^{-7} (6.34×10^{-8})	2.11×10^{-7} (9.36×10^{-8})	1.89×10^{-7} (5.25×10^{-8})	2.00×10^{-7} (1.15×10^{-7})
Ba	ND	ND	2.22×10^{-7} (5.34×10^{-8})	ND

(b)	Stage 6 (1.0 µm)	Stage 7 (0.56 µm)	Stage 8 (0.31 µm)	Stage 9 (0.18 µm)
Na	2.41×10^{-7} (1.62×10^{-8})	2.70×10^{-7} (1.43×10^{-8})	2.67×10^{-7} (1.70×10^{-8})	3.11×10^{-7} (1.58×10^{-8})
Al	1.76×10^{-6} (1.05×10^{-6})	3.62×10^{-6} (5.67×10^{-7})	2.65×10^{-6} (3.10×10^{-7})	ND
K	ND	ND	7.41×10^{-9} (9.36×10^{-10})	3.70×10^{-9} (1.18×10^{-9})
V	8.04×10^{-7} (1.61×10^{-9})	8.15×10^{-7} (1.63×10^{-9})	1.11×10^{-6} (1.11×10^{-8})	8.44×10^{-7} (5.06×10^{-9})
Cr	2.22×10^{-8} (1.14×10^{-8})	1.11×10^{-7} (2.91×10^{-8})	4.17×10^{-6} (5.83×10^{-8})	1.25×10^{-6} (1.78×10^{-7})
Mn	1.39×10^{-5} (2.64×10^{-7})	ND	ND	ND
Fe	ND	ND	8.15×10^{-8} (1.16×10^{-8})	ND
Ni	4.26×10^{-6} (2.38×10^{-7})	4.58×10^{-6} (5.04×10^{-8})	5.12×10^{-6} (7.68×10^{-8})	4.36×10^{-6} (9.60×10^{-8})
Zn	6.69×10^{-6} (2.74×10^{-7})	1.98×10^{-6} (1.09×10^{-7})	2.16×10^{-5} (3.02×10^{-7})	1.44×10^{-7} (1.33×10^{-7})
As	ND	ND	ND	ND
Se	1.33×10^{-7} (4.74×10^{-8})	3.70×10^{-8} (2.35×10^{-8})	1.41×10^{-7} (9.84×10^{-9})	5.56×10^{-8} (3.00×10^{-8})
Ba	3.85×10^{-7} (1.15×10^{-8})	3.41×10^{-7} (6.00×10^{-8})	ND	3.74×10^{-7} (1.54×10^{-8})

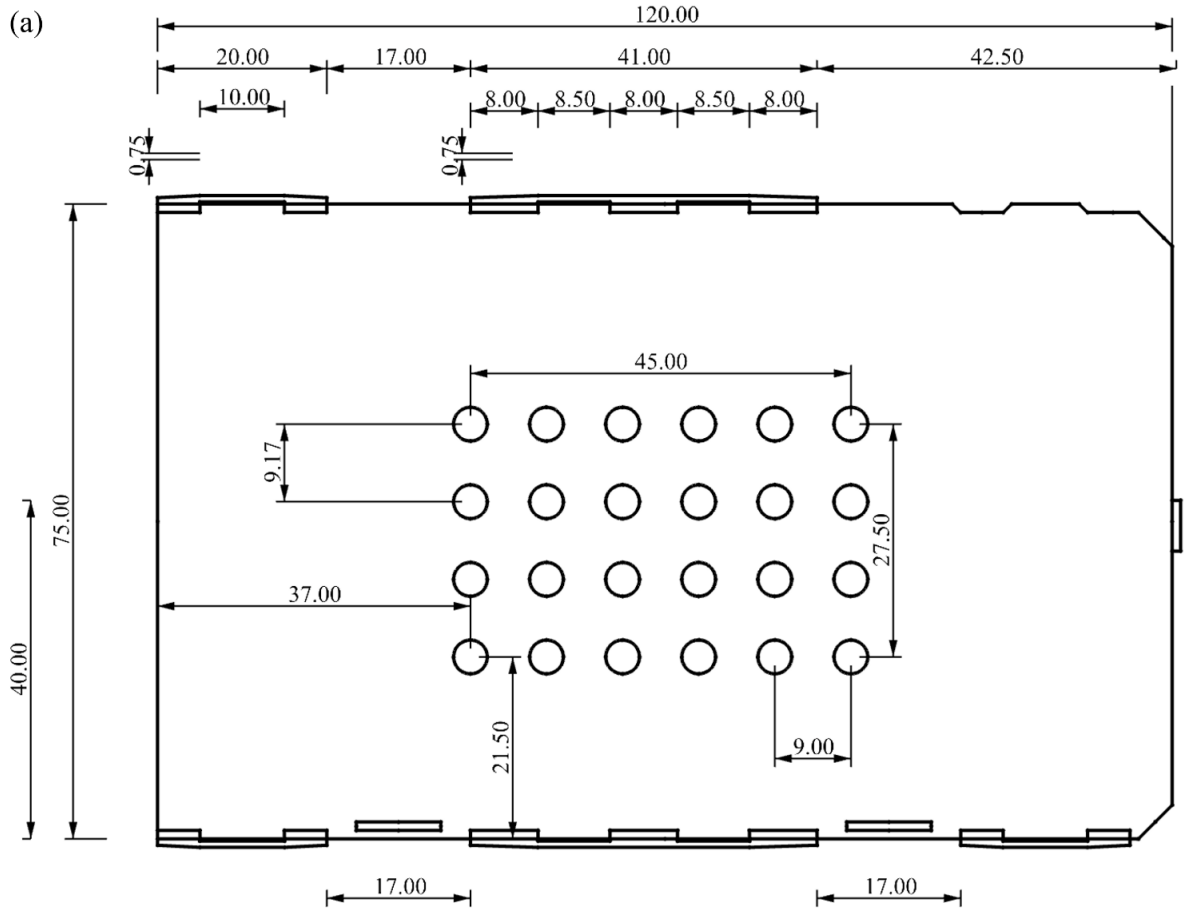
(a)
120.00
20.00
17.00
41.00
42.50
10.00
8.00
8.50
8.00
8.50
8.00
0.75
0.75
45.00
9.17
27.50
75.00
37.00
40.00
21.50
9.00
17.00
17.00

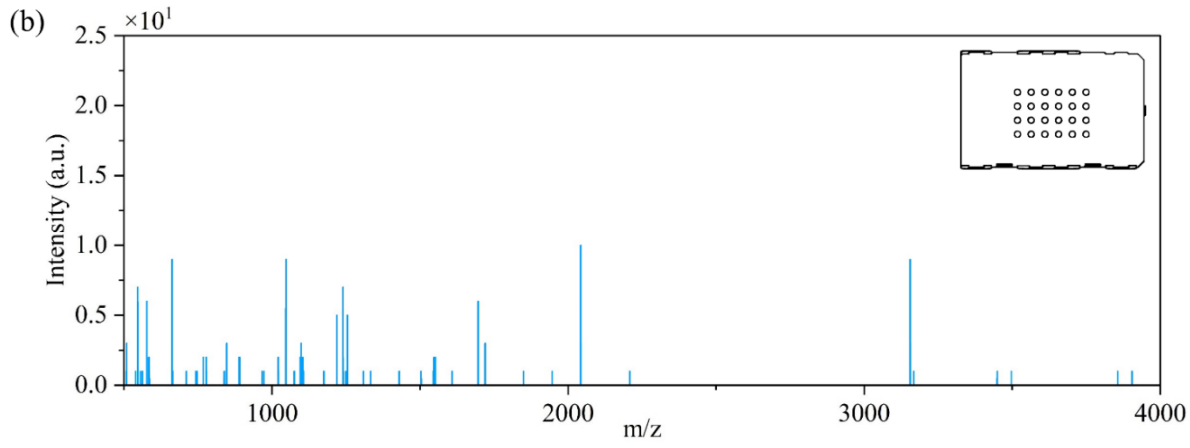
(b)
×10¹
2.5
2.0
1.5
1.0
0.5
0.0
Intensity (a.u.)
1000
2000
3000
4000
m/z

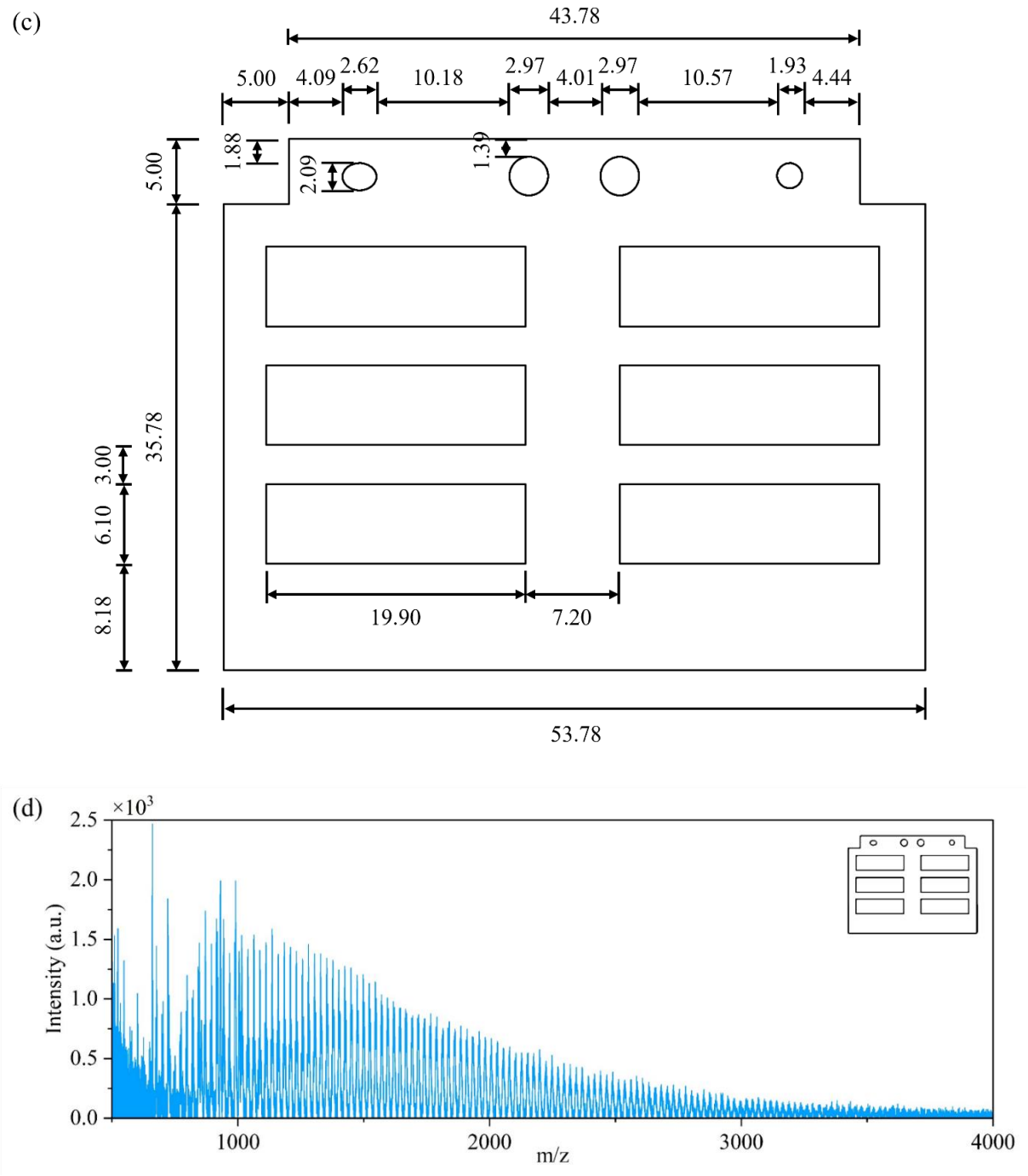

Figure S1 | Configurations of different 3D-printed HoLDI targets and corresponding mass spectra of the same aerosol sample acquired in pre-testing. (a) The first version prototype features an array of circular structures, resulting in weak intensity signals (magnitude = 10^1) as shown in (b). The size and shape of the plate are based on the Prespotted AnchorChip 96 target from Bruker Daltonics. (c) The second version includes larger rectangular windows instead of round hollows, producing improved signals (magnitude = 10^3) as presented in (d). The shape and size of the second plate are based on MSP 96 NALDI Target from Bruker Daltonics. Dimensions in (a) and (c) are labeled in millimeters (mm).

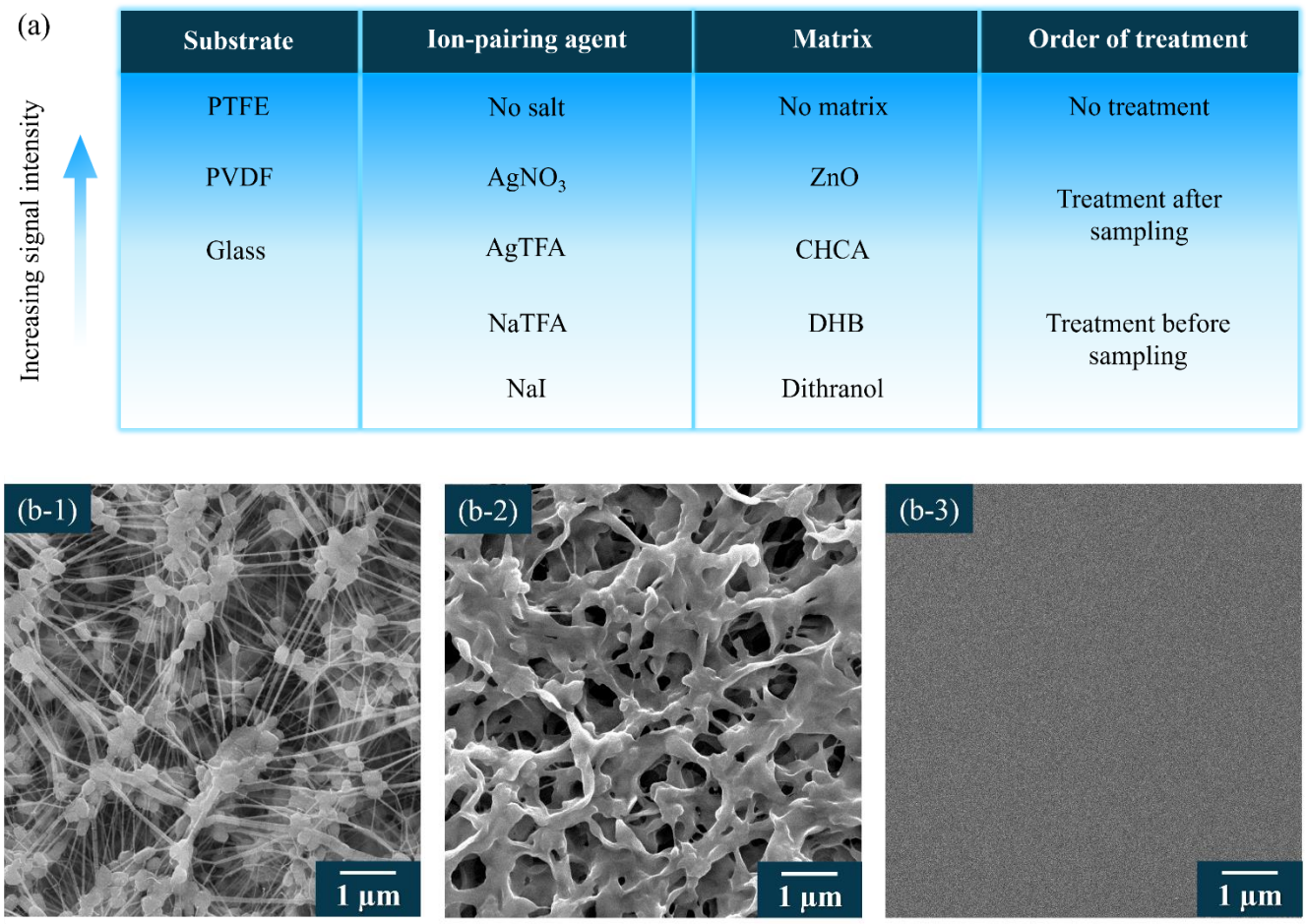

Figure S2 | Distinct analysis efficiencies for the use of different substrates, ion-pairing agents, matrices, and treatment processes. Analysis efficiencies are expressed as relative signal intensities. (a) The efficiencies in descending order for: i) Substrates, with polytetrafluoroethylene (PTFE) membrane > polyvinylidene fluoride (PVDF) membrane > glass; ii) Ion-pairing agents, with no salt > silver nitrate > silver trifluoroacetate (AgTFA) > sodium trifluoroacetate (NaTFA) > sodium iodide; iii) Matrices, with no matrix > zinc oxide nanoparticles > α-cyano-4-hydroxycinnamic acid (CHCA) > 2,3-dihydroxybenzoic acid (DHB) > dithranol; and iv) Treatment processes, with no treatment > applying matrices and salts on top of collected aerosol samples > depositing matrices and salts on blank substrates prior to sampling. (b-1) – (b-3) The surface structures of the PTFE membrane, PVDF membrane, and glass chip, respectively, acquired using scanning electron microscopy (SEM) with 10000× magnification.

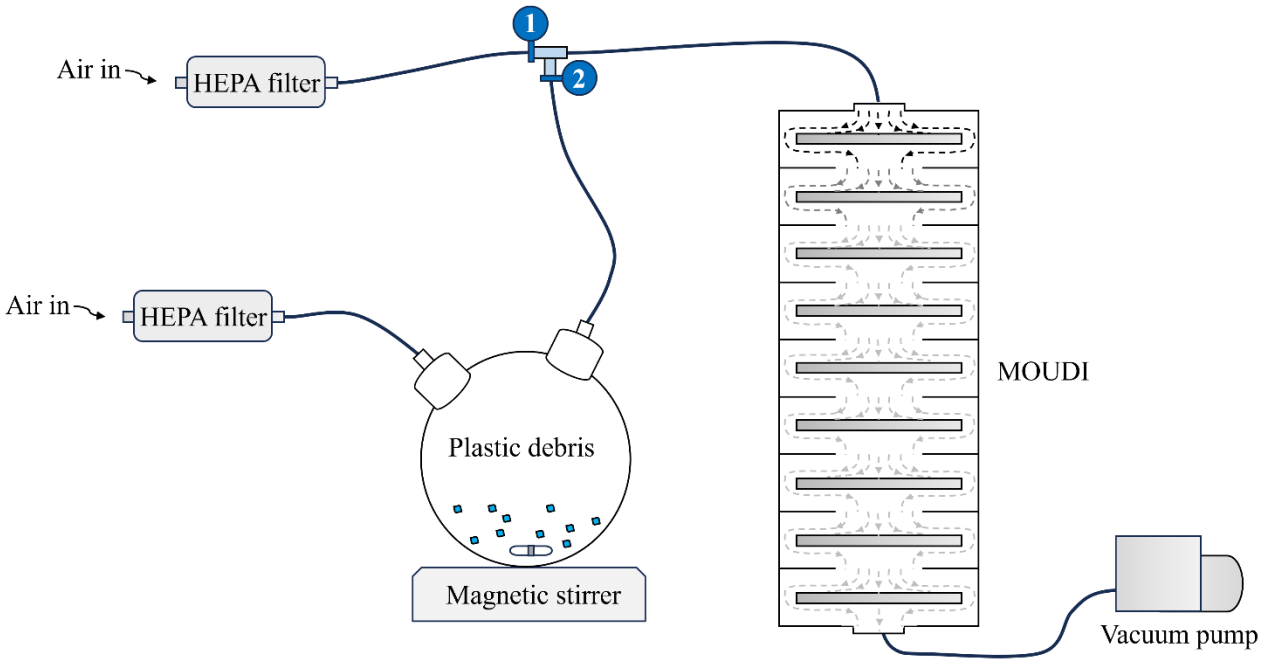

Figure S3 | The aerosol sampling setup for experiment blanks and positive controls. Collected air samples are analyzed using MALDI mass spectrometry to demonstrate the feasibility of the HoLDI target for airborne nano/microplastic detection. Air is passed through a micro-orifice uniform deposit impactor (MOUDI) using a vacuum pump and collected on substrates clamped onto MOUDI stages. For blanks, only valve 1 is open, allowing air in a cleanroom to be pumped into the sampling system, passed through a high efficiency particulate air (HEPA) filter unit, and collected on substrates by MOUDI. For spiked experiments, both valve 1 and valve 2 are open, allowing filtered cleanroom air to aerosolize micro/nanoplastic particles in a glass chamber and deposit airborne micro/nanoplastics onto substrates in MOUDI. Magnetic stirring aids in the generation and aerosolization of nano- and microplastic particles. The figure is not drawn to scale.

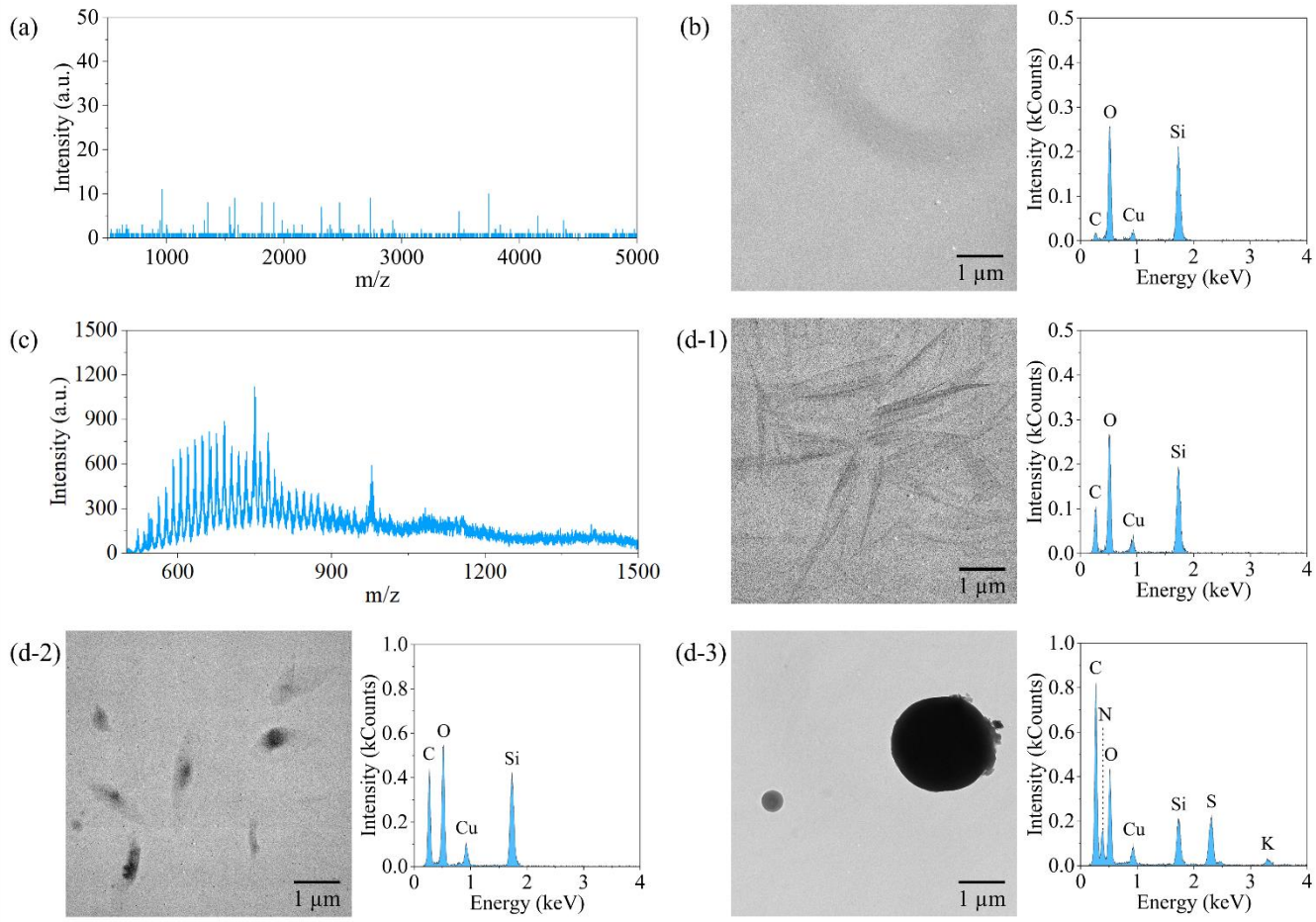

Figure S4 | Mass spectrometry (MS), transmission electron microscopy (TEM), and energy-dispersive X-ray spectroscopy (EDS) results of spiked experiments and blanks. (a) MS and (b) TEM-EDS data of one of the procedural blanks, showing no signals of plastic particles. (c) The mass spectrum of clean air spiked with PE form aerosols collected during positive controls, presenting signals of PE with mass differences of 28 Da. (d-1) – (d-3) TEM images of aerosols generated from PE forms, displaying three types of dominant structures. Elemental compositions of the generated aerosols exhibit increased carbon signal intensities, corresponding to plastic carbon backbones.

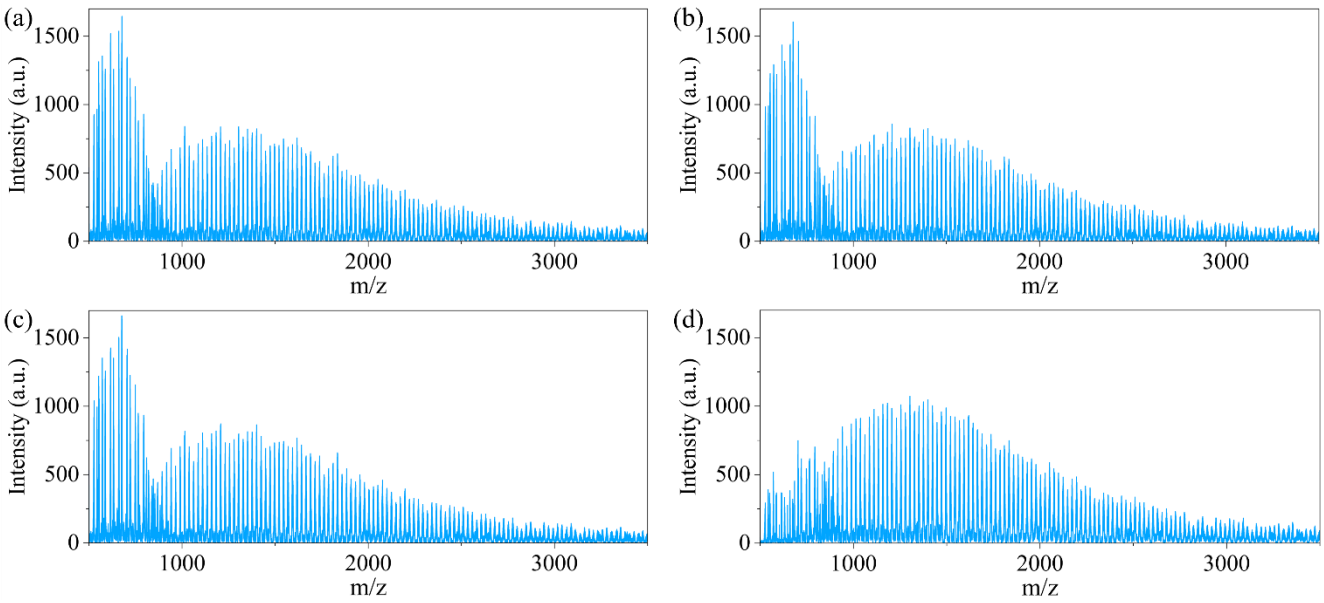

(e)	PEG, Na^+		PEG, K^+		PAHs							
	m/z	Intensity (a.u.)	m/z	Intensity (a.u.)	m/z	Intensity (a.u.)	m/z	Intensity (a.u.)	m/z	Intensity (a.u.)	m/z	Intensity (a.u.)
Replicate (a)	528.222	903.301	544.237	966.493	1182.906	794.639	1352.073	820.720	1520.955	700.399	1690.651	656.640
	572.006	1355.462	588.001	1258.832	1207.015	836.314	1376.986	793.043	1545.149	748.465	1714.009	573.196
	616.497	1518.894	632.799	1257.642	1232.147	771.282	1401.008	822.201	1569.806	688.088	1739.263	583.583
	661.012	1536.796	677.105	1637.339	1255.950	709.526	1425.095	782.847	1593.288	706.016	1763.209	495.974
	705.391	1345.033	721.496	1161.269	1280.609	675.189	1448.760	660.361	1617.872	755.688	1786.434	550.205
	748.978	1131.116	765.860	880.584	1304.609	816.059	1472.628	674.733	1641.672	674.050	1811.019	623.357
	794.884	889.554	809.648	595.125	1328.880	748.184	1496.651	712.076	1665.181	640.194	1835.351	639.657
Replicate (b)	527.887	983.221	543.570	871.370	1183.204	797.675	1353.005	725.008	1521.043	703.617	1690.995	665.416
	572.887	1289.494	588.535	1220.870	1207.320	823.328	1377.040	814.886	1545.848	747.270	1715.325	555.218
	616.416	1435.170	632.253	1316.831	1232.073	676.388	1400.260	823.847	1568.924	642.601	1739.332	554.809
	660.525	1430.602	676.621	1605.107	1255.428	731.619	1425.123	761.661	1594.202	680.381	1763.358	517.710
	705.323	1406.951	720.910	1110.351	1280.259	752.806	1449.679	682.059	1617.731	736.626	1787.596	521.610
	749.122	1039.359	765.983	911.767	1304.446	828.474	1472.920	749.748	1642.207	693.847	1810.680	617.634
	794.746	914.131	809.362	622.506	1328.011	750.106	1497.033	750.103	1665.669	682.075	1835.319	596.800
Replicate (c)	527.999	1023.776	544.282	994.828	1183.216	818.772	1351.741	814.245	1521.848	737.118	1690.134	653.883
	572.088	1352.501	588.292	1257.407	1207.458	857.787	1376.193	812.297	1545.701	730.243	1714.389	595.678
	617.216	1425.999	632.538	1351.433	1231.806	732.512	1400.438	864.008	1569.809	705.702	1738.685	635.452
	661.246	1495.885	677.001	1629.979	1255.083	726.747	1425.524	780.398	1593.962	696.643	1763.477	498.245
	705.680	1416.775	721.680	1225.484	1280.292	756.181	1449.066	692.135	1617.382	767.736	1787.199	544.420
	749.576	1155.190	765.309	937.378	1304.660	793.130	1472.400	705.286	1641.366	715.925	1811.610	584.261
	794.056	934.226	809.788	623.387	1327.873	758.032	1496.226	732.389	1666.885	636.670	1835.404	653.230
Average integrated	1230.259 ± 18.199		1097.569 ± 20.872		695.998 ± 6.375							

intensity (a.u.)			

Figure S5 | The reproducibility of HoLDI in analyzing real-world aerosol samples and a comparison between HoLDI and MALDI results. (a) – (c) Mass spectra of three separate subsamples of the same real-world aerosol sample obtained from the same filter substrate, analyzed using HoLDI-TOF-MS. Signals corresponding to sodium and potassium adducted polyethylene glycols (PEGs) and polycyclic aromatic hydrocarbons (PAHs) are consistently observed across all three spectra within the same mass range and with comparable signal intensities. (d) The mass spectrum of a subsample of the same real-world aerosol sample analyzed in (a) – (c), also taken from the same filter substrate, acquired using conventional MALDI-TOF-MS. PEG peaks are largely weakened in the MALDI spectrum. Tabulated in (e) are the m/z and signal intensity data for the detected PEGs and PAHs in the three subsamples, along with the calculated average integrated intensity and standard deviation values for the corresponding contaminants.

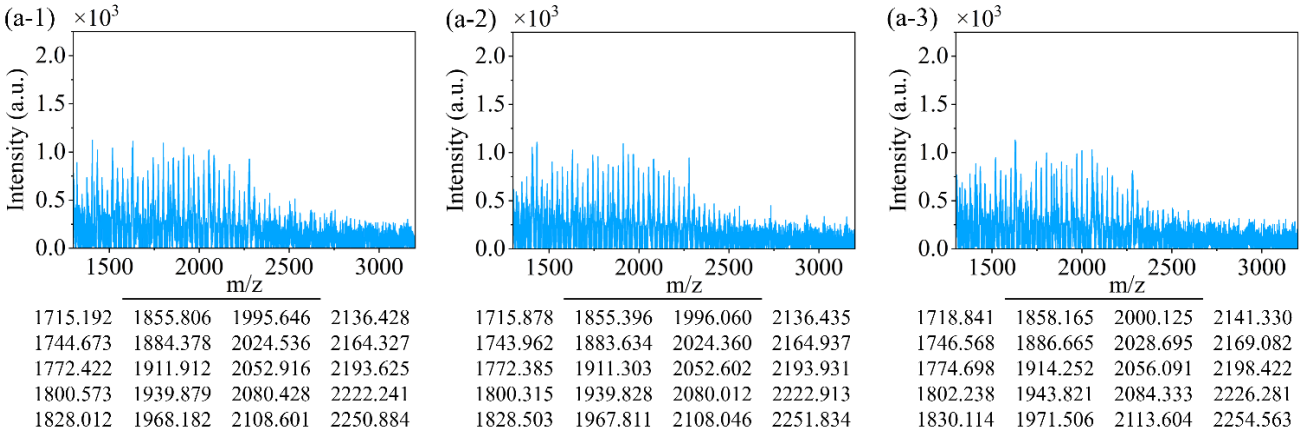

1715.192	1855.806	1995.646	2136.428
1744.673	1884.378	2024.536	2164.327
1772.422	1911.912	2052.916	2193.625
1800.573	1939.879	2080.428	2222.241
1828.012	1968.182	2108.601	2250.884

1715.878	1855.396	1996.060	2136.435
1743.962	1883.634	2024.360	2164.937
1772.385	1911.303	2052.602	2193.931
1800.315	1939.828	2080.012	2222.913
1828.503	1967.811	2108.046	2251.834

1718.841	1858.165	2000.125	2141.330
1746.568	1886.665	2028.695	2169.082
1774.698	1914.252	2056.091	2198.422
1802.238	1943.821	2084.333	2226.281
1830.114	1971.506	2113.604	2254.563

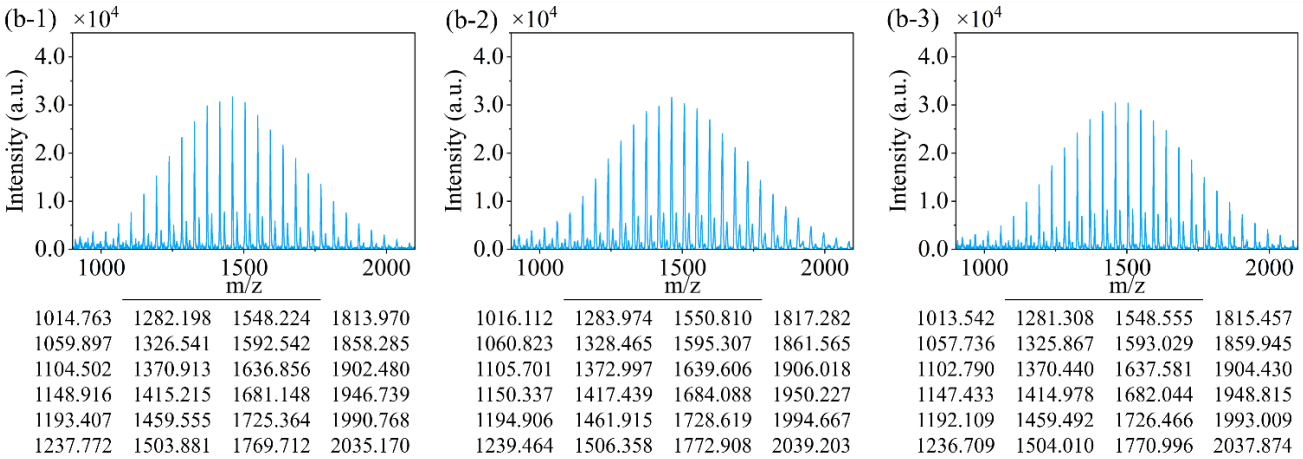

1014.763	1282.198	1548.224	1813.970
1059.897	1326.541	1592.542	1858.285
1104.502	1370.913	1636.856	1902.480
1148.916	1415.215	1681.148	1946.739
1193.407	1459.555	1725.364	1990.768
1237.772	1503.881	1769.712	2035.170

1016.112	1283.974	1550.810	1817.282
1060.823	1328.465	1595.307	1861.565
1105.701	1372.997	1639.606	1906.018
1150.337	1417.439	1684.088	1950.227
1194.906	1461.915	1728.619	1994.667
1239.464	1506.358	1772.908	2039.203

1013.542	1281.308	1548.555	1815.457
1057.736	1325.867	1593.029	1859.945
1102.790	1370.440	1637.581	1904.430
1147.433	1414.978	1682.044	1948.815
1192.109	1459.492	1726.466	1993.009
1236.709	1504.010	1770.996	2037.874

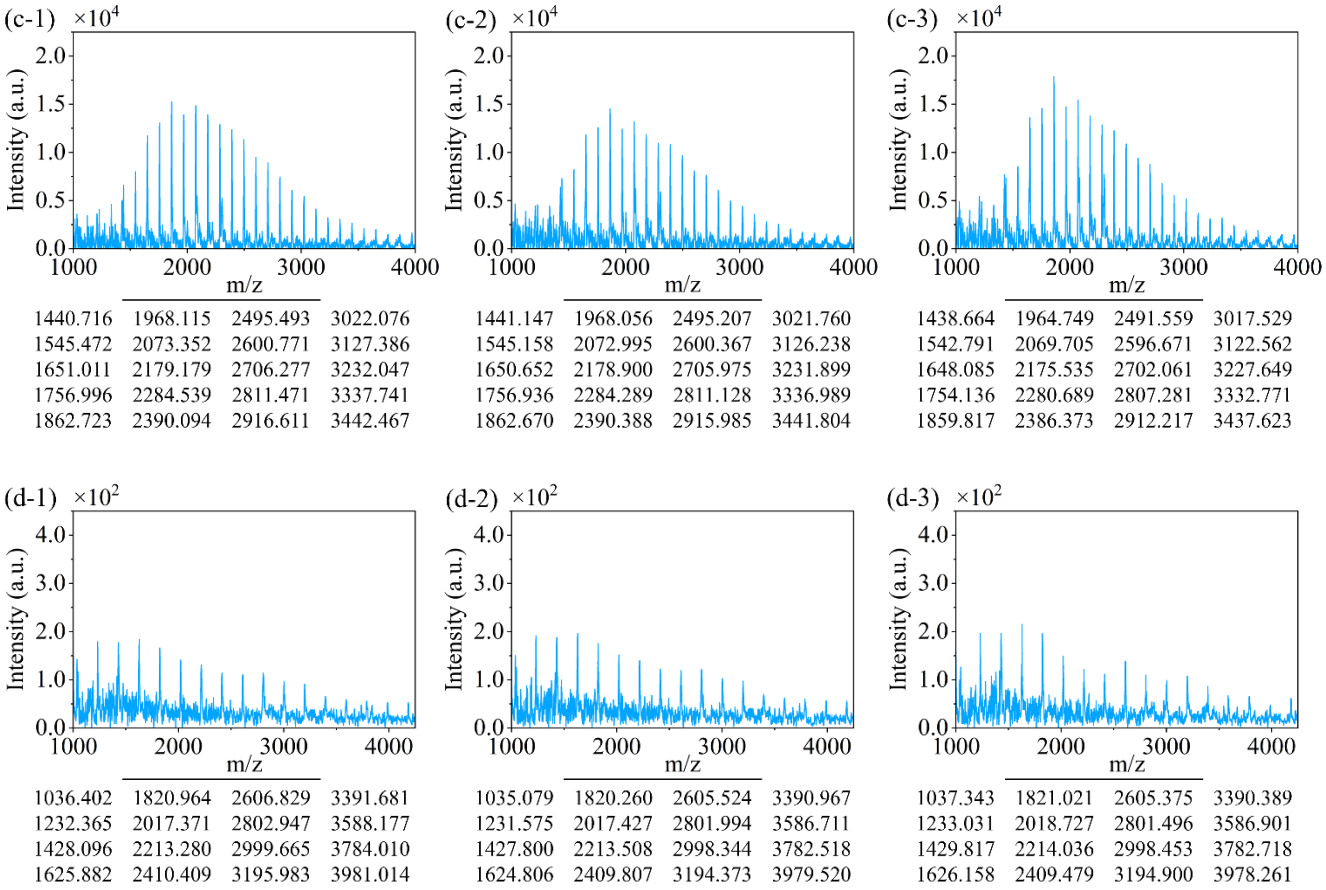

1440.716	1968.115	2495.493	3022.076
1545.472	2073.352	2600.771	3127.386
1651.011	2179.179	2706.277	3232.047
1756.996	2284.539	2811.471	3337.741
1862.723	2390.094	2916.611	3442.467

1441.147	1968.056	2495.207	3021.760
1545.158	2072.995	2600.367	3126.238
1650.652	2178.900	2705.975	3231.899
1756.936	2284.289	2811.128	3336.989
1862.670	2390.388	2915.985	3441.804

1438.664	1964.749	2491.559	3017.529
1542.791	2069.705	2596.671	3122.562
1648.085	2175.535	2702.061	3227.649
1754.136	2280.689	2807.281	3332.771
1859.817	2386.373	2912.217	3437.623

1036.402	1820.964	2606.829	3391.681
1232.365	2017.371	2802.947	3588.177
1428.096	2213.280	2999.665	3784.010
1625.882	2410.409	3195.983	3981.014

1035.079	1820.260	2605.524	3390.967
1231.575	2017.427	2801.994	3586.711
1427.800	2213.508	2998.344	3782.518
1624.806	2409.807	3194.373	3979.520

1037.343	1821.021	2605.375	3390.389
1233.031	2018.727	2801.496	3586.901
1429.817	2214.036	2998.453	3782.718
1626.158	2409.479	3194.900	3978.261

Figure S6 | The reproducibility of HoLDI in analyzing selected nano/microplastic standards spiked into real-world aerosol samples, including (a) polyethylene (PE), (b) polyethylene glycol (PEG), (c) polystyrene (PS), and (d) polyethylene terephthalate (PET).

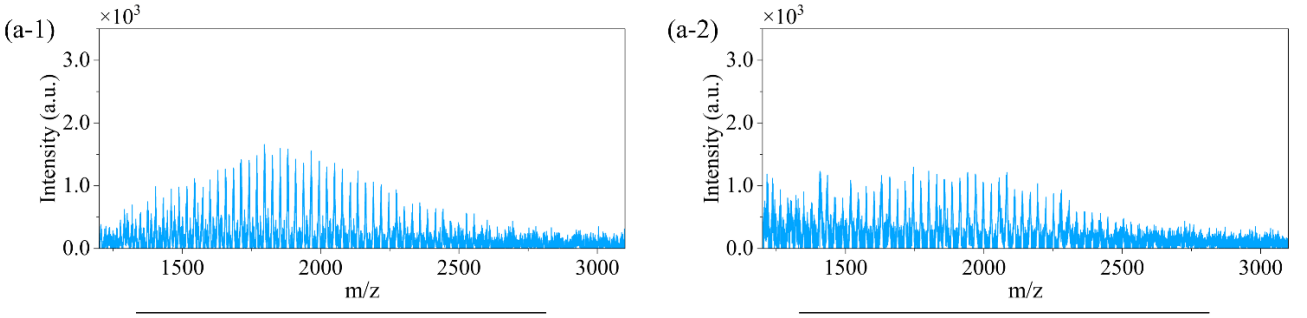

1544.562	1685.557	1826.062	1966.256	2106.954	2246.444
1573.078	1713.318	1854.297	1994.366	2134.488	2274.843
1600.744	1741.663	1881.669	2022.566	2162.665	2302.763
1628.897	1769.821	1909.745	2050.501	2190.817	2330.959
1657.491	1797.731	1938.243	2078.234	2218.309	2359.014

1629.809	1744.346	1855.787	1968.748	2080.901	2192.835
1659.711	1771.871	1884.280	1996.811	2109.293	2223.857
1687.320	1799.939	1912.533	2025.246	2138.428	2252.744
1715.372	1827.809	1940.602	2052.610	2165.382	2277.700

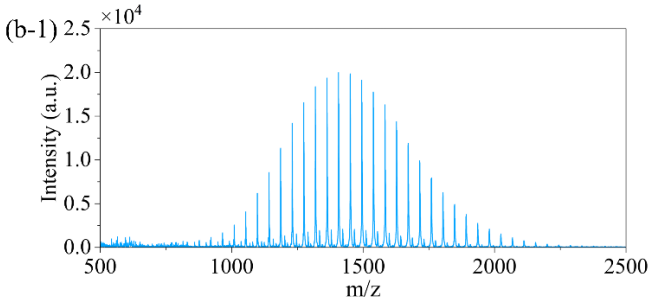

921.522	1142.212	1362.717	1583.096	1803.326	2023.348
965.677	1186.326	1406.803	1627.152	1847.343	2067.243
1009.835	1230.434	1450.883	1671.197	1891.226	2111.197
1053.964	1274.533	1494.957	1715.241	1935.362	2155.281
1098.094	1318.631	1539.027	1759.292	1979.357	2199.033

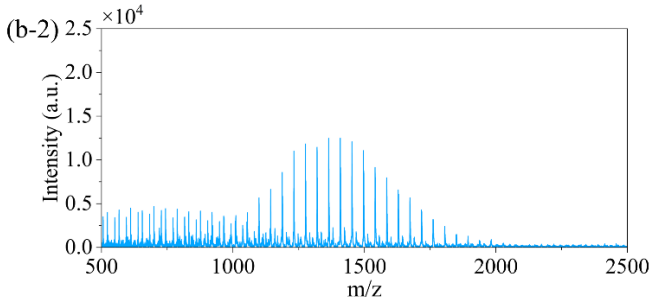

1054.981	1231.613	1408.155	1584.562	1760.867
1098.757	1275.764	1452.264	1628.651	1804.932
1143.317	1319.884	1496.385	1672.758	1848.990
1187.468	1364.027	1540.474	1716.812	1893.195

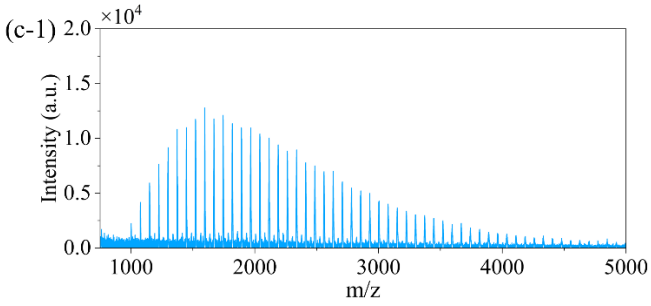

1000.955	1520.636	2039.791	2557.907	3075.396	3594.449
1074.575	1594.830	2113.802	2631.654	3149.003	3668.710
1148.938	1669.141	2187.910	2705.698	3223.797	3742.659
1223.794	1743.162	2261.936	2779.737	3298.028	3816.801
1298.091	1817.445	2335.952	2853.761	3372.843	3891.396
1372.247	1891.603	2409.912	2927.568	3446.855	3965.329
1446.476	1965.675	2483.814	3001.577	3520.269	4039.181

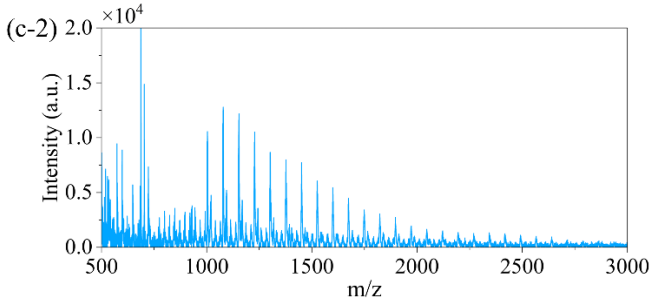

928.983	1375.827	1821.012	2267.277
1002.720	1449.970	1895.290	2341.945
1077.315	1523.968	1969.688	2415.800
1152.424	1598.295	2044.482	2490.618
1227.004	1672.524	2118.734	2564.715
1301.034	1746.823	2192.993	2638.591

Figure S7 | Examination of potential m/z shifts in plastic signals in the presence of complex airborne particles. (a-1), (b-1), and (c-1) present the mass spectra of polyethylene (PE), polyethylene glycol (PEG), and polydimethylsiloxane (PDMS) standards analyzed using conventional MALDI with a stainless-steel target plate. (a-2), (b-2), and (c-2) present the mass spectra of PE, PEG, and PDMS standards spiked onto substrates containing real-world aerosol samples, analyzed using HoLDI. Characteristic polymer peaks are tabulated below the mass spectra. Only the m/z values of the dominant peak series are listed.

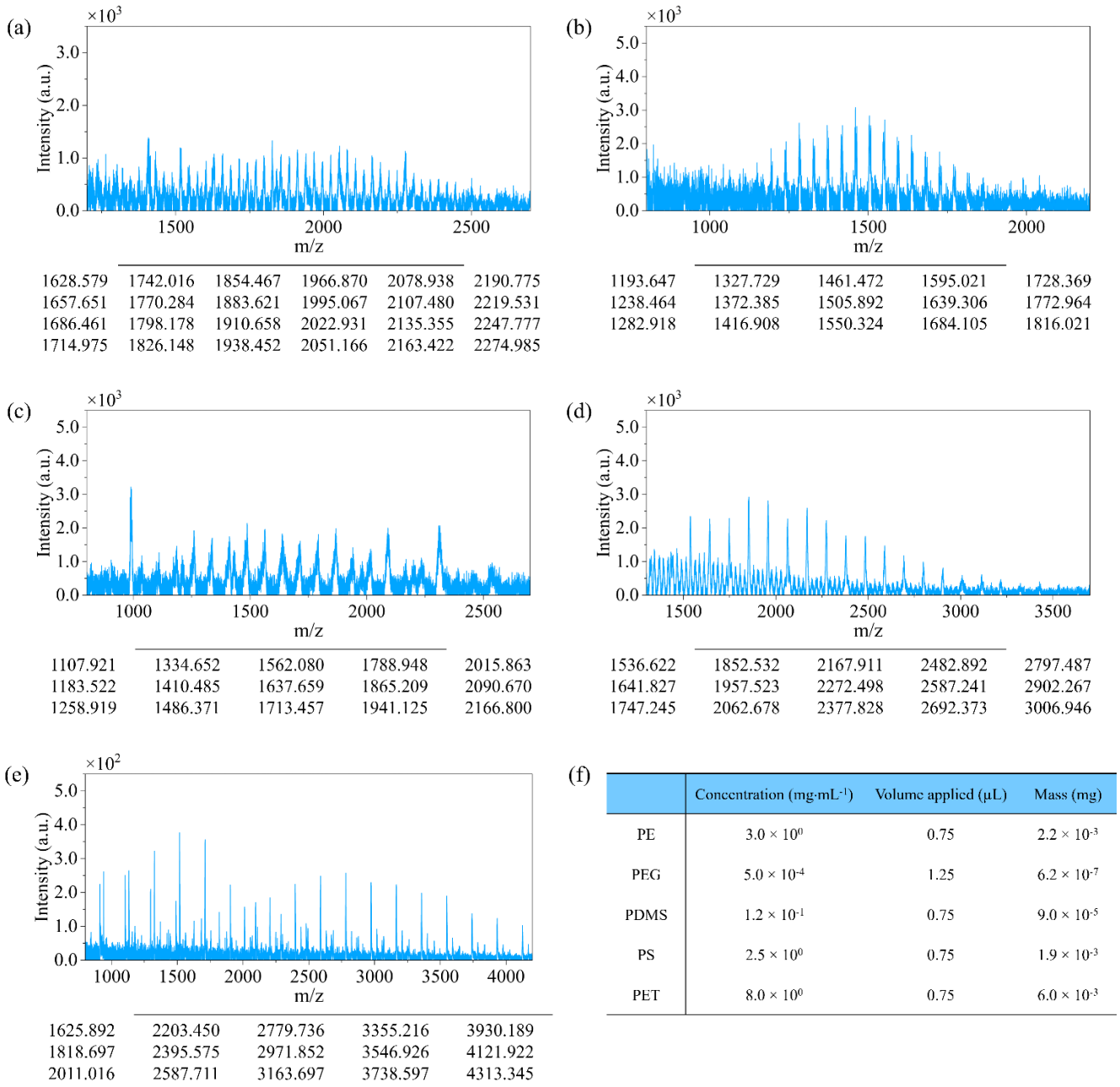

	Concentration (mg·mL^{-1})	Volume applied (μL)	Mass (mg)
PE	3.0×10^{0}	0.75	2.2×10^{-3}
PEG	5.0×10^{-4}	1.25	6.2×10^{-7}
PDMS	1.2×10^{-1}	0.75	9.0×10^{-5}
PS	2.5×10^{0}	0.75	1.9×10^{-3}
PET	8.0×10^{0}	0.75	6.0×10^{-3}

Figure S8 | Limits of detection of HoLDI-TOF-MS for commonly used plastics in the presence of real-world aerosol samples. The mass spectra of the lowest detectable concentration for the plastics (a) polyethylene (PE), (b) polyethylene glycol (PEG), (c) polydimethylsiloxane (PDMS), (d) polystyrene (PS), and (e) polyethylene terephthalate (PET), along with their corresponding characteristic peaks. The limits of detection of studied plastics are summarized in (f).

Supplementary References

1. González-Pleiter, M., et al., Occurrence and transport of microplastics sampled within and above the planetary boundary layer. Science of The Total Environment, 2021. 761: 143213.
2. Trainic, M., et al., Airborne microplastic particles detected in the remote marine atmosphere. Communications Earth & Environment, 2020. 1(1): 64.
3. Tian, L., et al., Quantification of polyethylene terephthalate microplastics and nanoplastics in sands, indoor dust and sludge using a simplified in-matrix depolymerization method. Marine Pollution Bulletin, 2022. 175: 113403.
4. Liu, C., et al., Widespread distribution of PET and PC microplastics in dust in urban China and their estimated human exposure. Environment International, 2019. 128: 116-124.
5. Xie, L., et al., Automatic identification of individual nanoplastics by Raman spectroscopy based on machine learning. Environmental Science & Technology, 2023. 57(46): 18203-18214.
6. Wang, Z., et al., Advances in ultra-trace analytical capability for micro/nanoplastics and water-soluble polymers in the environment: Fresh falling urban snow. Environmental Pollution, 2021. 276: 116698.
7. Mani, T., et al., Microplastics profile along the Rhine River. Scientific Reports, 2015. 5: 17988.
8. Barrows, A. P. W., et al., A watershed-scale, citizen science approach to quantifying microplastic concentration in a mixed land-use river. Water Research, 2018. 147: 382-392.
9. Hendrickson, E., et al., Microplastic abundance and composition in western Lake Superior as determined via microscopy, Pyr-GC/MS, and FTIR. Environmental Science & Technology, 2018. 52(4): 1787-1796.
10. Materić, D., et al., Presence of nanoplastics in rural and remote surface waters. Environmental Research Letters, 2022. 17(5): 054036.
11. Ter Halle, A., et al., Nanoplastic in the North Atlantic subtropical gyre. Environmental Science & Technology, 2017. 51(23): 13689-13697.
12. Savoca, S., et al., Microplastics occurrence in the Tyrrhenian waters and in the gastrointestinal tract of two congener species of seabreams. Environmental Toxicology and Pharmacology, 2019. 67: 35-41.
13. Samandra, S., et al., Microplastic contamination of an unconfined groundwater aquifer in Victoria, Australia. Science of The Total Environment, 2022. 802: 149727.
14. Panno, S. V., et al., Microplastic contamination in karst groundwater systems. Ground Water, 2019. 57(2): 189-196.
15. Fuller, S. and Gautam, A., A procedure for measuring microplastics using pressurized fluid extraction. Environmental Science & Technology, 2016. 50(11): 5774-80.
16. Nematollahi, M. J., et al., Microplastic occurrence in urban and industrial soils of Ahvaz metropolis: A city with a sustained record of air pollution. Science of The Total Environment, 2022. 819: 152051.
17. Corradini, F., et al., Evidence of microplastic accumulation in agricultural soils from sewage sludge disposal. Science of The Total Environment, 2019. 671: 411-420.
18. Wahl, A., et al., Nanoplastic occurrence in a soil amended with plastic debris. Chemosphere, 2021. 262: 127784.
19. Mazariegos-Ortíz, C., et al., First evidence of microplastic pollution in the El Quetzalito sand beach of the Guatemalan Caribbean. Marine Pollution Bulletin, 2020. 156: 111220.
20. Eo, S., et al., Abundance, composition, and distribution of microplastics larger than 20 mum in sand beaches of South Korea. Environmental Pollution, 2018. 238: 894-902.
21. Tibbetts, J., et al., Abundance, distribution, and drivers of microplastic contamination in urban river environments. Water, 2018. 10(11): 1597.

22. Castañeda, R. A., et al., Microplastic pollution in St. Lawrence River sediments. Canadian Journal of Fisheries and Aquatic Sciences, 2014. 71(12): 1767-1771.
23. Fialova, J., et al., Three-dimensional printed target plates for matrix-assisted laser desorption/ionization mass spectrometry. Analytical Chemistry, 2020. 92(19): 12783-12788.
24. Wang, D., et al., 3D printing of graphene-doped target for "matrix-free" laser desorption/ionization mass spectrometry. Chemical Communications, 2018. 54(22): 2723-2726.